PNAS RESEARCH ARTICLE | PLANT BIOLOGY

Modulation of xanthophyll cycle impacts biomass productivity in the marine microalga *Nannochloropsis*

Giorgio Perin[a,1], Alessandra Bellan[a,1], Tim Michelberger[a], Dagmar Lyska[b], Setsuko Wakao[b], Krishna K. Niyogi[b,c,d], and Tomas Morosinotto[a,2]

Edited by Donald Ort, University of Illinois at Urbana Champaign, Urbana, IL; received August 17, 2022; accepted May 15, 2023

Life on earth depends on photosynthetic primary producers that exploit sunlight to fix CO_2 into biomass. Approximately half of global primary production is associated with microalgae living in aquatic environments. Microalgae also represent a promising source of biomass to complement crop cultivation, and they could contribute to the development of a more sustainable bioeconomy. Photosynthetic organisms evolved multiple mechanisms involved in the regulation of photosynthesis to respond to highly variable environmental conditions. While essential to avoid photodamage, regulation of photosynthesis results in dissipation of absorbed light energy, generating a complex trade-off between protection from stress and light-use efficiency. This work investigates the impact of the xanthophyll cycle, the light-induced reversible conversion of violaxanthin into zeaxanthin, on the protection from excess light and on biomass productivity in the marine microalgae of the genus *Nannochloropsis*. Zeaxanthin is shown to have an essential role in protection from excess light, contributing to the induction of nonphotochemical quenching and scavenging of reactive oxygen species. On the contrary, the overexpression of zeaxanthin epoxidase enables a faster reconversion of zeaxanthin to violaxanthin that is shown to be advantageous for biomass productivity in dense cultures in photobioreactors. These results demonstrate that zeaxanthin accumulation is critical to respond to strong illumination, but it may lead to unnecessary energy losses in light-limiting conditions and accelerating its reconversion to violaxanthin provides an advantage for biomass productivity in microalgae.

microalgae | xanthophyll cycle | photosynthesis engineering | nonphotochemical quenching | photobioreactor

Significance

This work investigates the impact of the xanthophyll cycle in marine microalgae on the trade-off between photoprotection and light-use efficiency. Our results demonstrate that while zeaxanthin is essential for photoprotection upon exposure to strong illumination, it leads to unnecessary energy losses in light-limiting conditions and thus accelerating its reconversion to violaxanthin provides an advantage for biomass productivity in microalgae in dense cultures.

Photosynthetic organisms are the main primary producers on our planet, supporting the metabolism of most life forms, thanks to their ability to exploit sunlight to drive the fixation of CO_2 into biomass. Approximately half of global primary production is associated with aquatic environments and depends on microalgae, making these organisms essential to sustain life in natural ecosystems (1). Investigating the regulation of photosynthesis is essential both to understand the dynamics of primary productivity in natural ecosystems and to pave the way to improve light-to-biomass conversion efficiency and increase crop productivity to respond to an ever-increasing demand for food (2).

In the natural environment, light absorbed by photosynthetic pigments, such as chlorophyll (Chl), can easily become excessive with respect to the metabolic capacity of the cell, driving the overreduction of the photosynthetic electron transport chain and consequently the generation of toxic reactive oxygen species (ROS). Photosynthetic organisms evolved several mechanisms regulating light-use efficiency and photosynthetic electron transport to reduce the probability of overreduction and cell damage (3, 4). Among these mechanisms, nonphotochemical quenching (NPQ) drives the dissipation of excited states of Chl (i.e., Chl singlets) as heat, thus reducing the probability of generating ROS. In eukaryotes, NPQ depends both on the generation of a ΔpH across the thylakoid membrane and the presence of specific molecular activators, namely PsbS and/or LHCSR/LHCX, depending on the species (5, 6).

In most eukaryotic organisms, a second major regulatory mechanism of photosynthesis is the xanthophyll cycle. Upon exposure to excess irradiation, the decrease in pH of the thylakoid lumen induces the activation of violaxanthin de-epoxidase (VDE) that catalyzes the conversion of violaxanthin into zeaxanthin (7, 8). Zeaxanthin contributes to photoprotection both by enhancing NPQ and directly scavenging Chl triplets and ROS (9). In limiting light conditions, zeaxanthin is converted back to violaxanthin by zeaxanthin epoxidase (ZEP). The two reactions of the cycle have different kinetics and, while zeaxanthin accumulates in a few minutes after exposure to strong illumination, it takes tens of minutes for ZEP to convert it back to violaxanthin. This slower rate of reconversion has been suggested to provide more effective photoprotection in nature in case of repeated

Author contributions: T. Morosinotto designed research; G.P. and A.B. performed research; S.W. contributed new reagents/analytic tools; G.P., T. Morosinotto, and K.K.N. analyzed data; T. Michelberger data collection; D.L. and K.K.N. generation of the *N. oceanica* mutants; G.P., T. Morosinotto, and K.K.N. critical revision of data and manuscript; and G.P. and T. Morosinotto wrote the paper.

The authors declare no competing interest.

This article is a PNAS Direct Submission.

[1]G.P. and A.B. contributed equally to this work.

[2]To whom correspondence may be addressed. Email: tomas.morosinotto@unipd.it.

This article contains supporting information online at https://www.pnas.org/lookup/suppl/doi:10.1073/pnas.2214119120/-/DCSupplemental.

Published June 12, 2023.

peaks of excess irradiation due to rapidly changing weather conditions (10).

NPQ and the xanthophyll cycle are important to protect the photosynthetic apparatus from excess irradiation, and they have been shown to contribute to the fitness of photosynthetic organisms in dynamic natural conditions (11). On the contrary, their activity results in the dissipation of a fraction of absorbed energy (12), reducing light-to-biomass conversion efficiency. If constitutively active, thus, they can negatively impact biomass productivity in light-limiting conditions (13). The energy losses due to photosynthesis regulatory mechanisms can be particularly impactful in the case of light fluctuations, when NPQ and the xanthophyll cycle are activated during light peaks and remain active when the illumination decreases. In plants, it has been shown that accelerating the kinetics of the xanthophyll cycle can lead to a remarkable increase in photosynthetic productivity in the field (14, 15).

Unicellular algae, like all other photosynthetic organisms, are exposed to light fluctuations in nature and have multiple mechanisms to modulate their photosynthetic efficiency, including NPQ and the xanthophyll cycle (16, 17). Light dynamics are also highly impactful when microalgae are cultivated in photobioreactors for commercial applications, where culture optical density and its mixing generate additional light fluctuations, beyond the natural dynamics (18). In this work, we investigated the impact of the xanthophyll cycle in the heterokont marine microalgae *Nannochloropsis gaditana* (*N. gaditana*) and *N. oceanica*, showing the essential role of zeaxanthin in photoprotection from light stress but also demonstrating that a faster reconversion of zeaxanthin to violaxanthin improves biomass productivity in a light-limited environment, typical of dense cultures of industrial systems.

Results

Dynamics of Xanthophyll Composition in *Nannochloropsis*. *N. gaditana* cultures, exposed to different light intensities, showed accumulation of antheraxanthin and zeaxanthin following the increase in irradiance, with a corresponding reduction in the content of violaxanthin (Fig. 1*A*). It is worth noting that even when grown in limiting light conditions [i.e., < 150 µmol photons m^{-2} s^{-1}, (19)], *Nannochloropsis* cells showed a small but detectable presence of zeaxanthin (>2%, Fig. 1*A*), different from plants or other eukaryotic microalgae, where zeaxanthin is normally not detectable in low light (20). Cells exposed to high light (1,000 µmol photons m^{-2} s^{-1}) for different time intervals showed a progressive increase in antheraxanthin and zeaxanthin with a corresponding decrease in violaxanthin (Fig. 1*B* and *SI Appendix*, Table S1). Vaucheriaxanthin and β-carotene, the other major carotenoids detected, instead did not change in response to the treatment with excess light (*SI Appendix*, Table S1), all results fully consistent with the activation of the xanthophyll cycle induced by the strong illumination. Antheraxanthin content reached a maximum after 15 min, while zeaxanthin accumulation continued to increase, not reaching a saturation even after 2 h of high light treatment (Fig. 1*B*).

Cells were also treated with extreme, nonphysiological, light intensity (4,000 µmol photons m^{-2} s^{-1} while also removing CO_2 supply, Fig. 1*C*), to maximize light excess. This resulted in a further

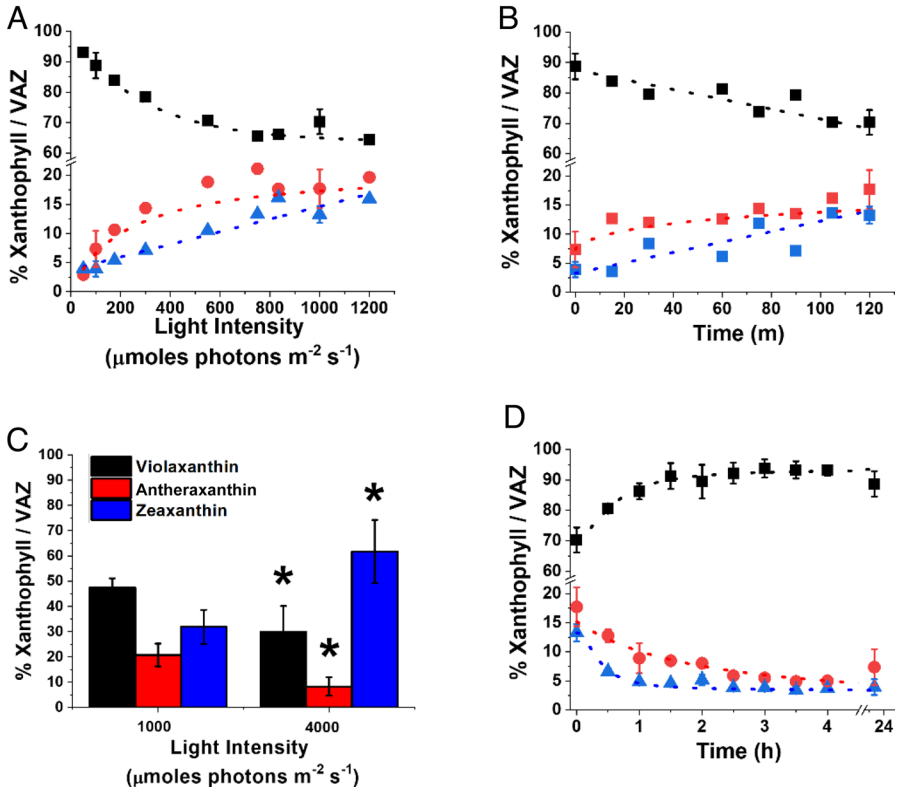

Fig. 1. Dynamic of xanthophyll cycle in *N. gaditana*. (*A*) Light dependence of xanthophylls accumulation in *N. gaditana* previously cultivated at 100 µmol photons m^{-2} s^{-1}. Cells were exposed for 2 h at the different light intensities. (*B*) Time dependence of xanthophylls accumulation after moving cells from 100 to 1,000 µmol photons $m^{-2}s^{-1}$. (*C*) The same *N. gaditana* cells were also exposed to extreme illumination (1,000 and 4,000 µmol photons m^{-2} s^{-1}) for 2 h, removing CO_2 to maximize photosynthesis saturation. (*D*) Time-dependent relaxation of xanthophylls after exposure at 1,000 µmol photons m^{-2} s^{-1} for 2 h, as in panel *B*. Data are fitted with logistic functions and are expressed as percentage of each xanthophyll molecule over their sum (violaxanthin, antheraxanthin, and zeaxanthin, VAZ). Black, violaxanthin; red, antheraxanthin; blue, zeaxanthin. Asterisks in panel *C* indicate statistically significant differences in the content of each xanthophyll molecule between 4,000 and 1,000 µmol photons m^{-2} s^{-1} (*t* test, *P*-value < 0.05). Data are expressed as average ± SD of three independent biological replicates.

accumulation of zeaxanthin that reached in the most extreme case 60% of the VAZ pool (Fig. 1*C*), showing that this organism has a very large reservoir of violaxanthin convertible to zeaxanthin.

To investigate xanthophyll cycle relaxation dynamics, *N. gaditana* cells treated with 1,000 µmol photons m^{-2} s^{-1} for 2 h to induce zeaxanthin biosynthesis were afterward exposed to dim light (Fig. 1*D*). Dim light was preferred to dark because the former is expected to increase the amount of photosynthesis products, such as O_2 and NADPH, that are required by the epoxidation reaction catalyzed by ZEP (21). Zeaxanthin and antheraxanthin synthesized during the high light treatment were fully reconverted to violaxanthin after approximately 4 h (Fig. 1*D*).

Impact of Xanthophyll Dynamics on Nonphotochemical Quenching. Exposure to saturating illumination also activates NPQ that can be quantified by monitoring chlorophyll fluorescence in vivo (see *Materials and Methods* for details). In *Nannochloropsis,* NPQ activation reaches saturation after approx. 10 min of exposure to saturating illumination (Fig. 2*A*). In *Nannochloropsis*, NPQ is strongly influenced by zeaxanthin synthesis, as shown by treatment with a VDE inhibitor (i.e., DTT) that causes a strong reduction of its activation (*SI Appendix*, Fig. S1).

The impact of zeaxanthin on NPQ can be assessed also by performing multiple NPQ induction measurements, separated by a dark relaxation (22, 23) (Fig. 2). In this protocol, most of NPQ relaxes after the first illumination step, following the dissipation of ΔpH across the thylakoid membrane. NPQ induction during the second illumination, however, is faster because some of the zeaxanthin accumulated is not completely reconverted in the dark interval (Fig. 2*B*). By changing the interval between the two illumination phases, it is possible to demonstrate that the pool of zeaxanthin synthesized during the first 8 min of light treatment takes much longer to be completely reconverted into violaxanthin, and its presence accelerates NPQ activation in a second light treatment even if this is separated from the first by 90 min in the dark (Fig. 2*C*). Changing instead the length of light treatment confirmed that zeaxanthin active in NPQ is quickly synthesized but then more slowly reconverted into violaxanthin. As example, only 2 min of illumination are sufficient to accumulate enough zeaxanthin to make NPQ faster in a second measurement after 10 min of dark treatment (Fig. 2*D*).

Generation of *Nannochloropsis* Strains with Altered Xanthophyll Cycle. To investigate the impact of the xanthophyll cycle on photoprotection mechanisms in *Nannochloropsis*, three independent *vde KO* strains were isolated via homology-directed repair mediated by CRISPR-Cpf1 technology (24, 25) (see *Materials and Methods* for details). Strains with impaired expression of the *VDE* gene (Phycocosm GENE ID: rna9604) were first selected by phenotypic screening via PAM-Imaging, looking for isolates with reduced NPQ capacity. The insertion of the resistance cassette in the expected genome locus was later validated by PCR (*SI Appendix*, Fig. S2).

Three independent strains overexpressing the *ZEP* gene (*ZEP* OE) were also isolated, after *Nannochloropsis* transformation with a modular vector for effective expression of genes of interest (see *SI Appendix, Materials and Methods* for details), into which the full endogenous *ZEP* gene (Gene ID: rna3613) was cloned. Transformed strains were screened phenotypically by PAM-Imaging, looking for those where NPQ relaxation in the dark was faster than that in WT, and RT-PCR was used to validate that they indeed overexpressed the *ZEP* gene (*SI Appendix*, Fig. S3).

These strains were compared to *lhcx1 KO* unable to activate NPQ (26) because of the absence of LHCX1 (Gene ID: rna606), a protein homologous to LHCX/LHCSR proteins, shown in

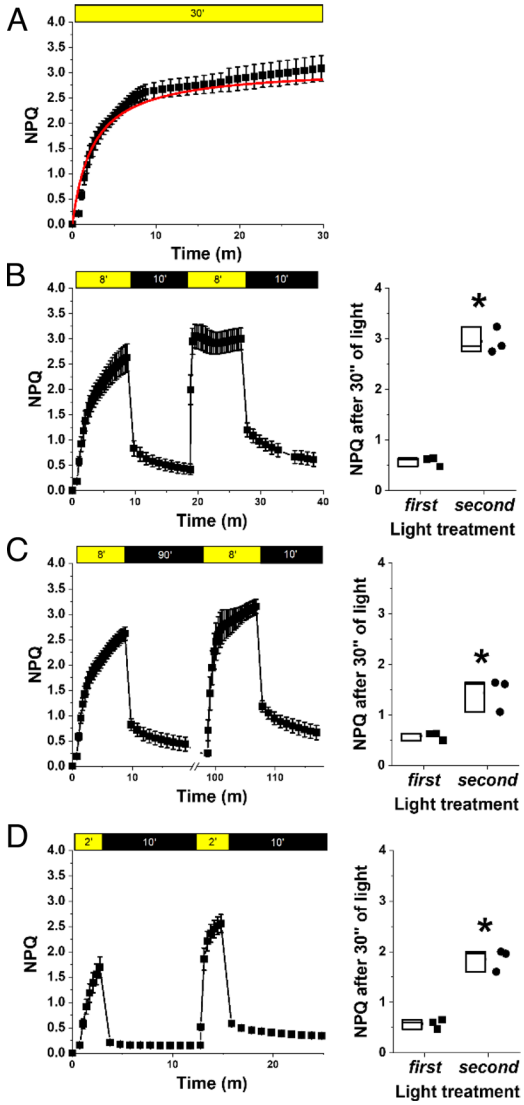

Fig. 2. Influence of zeaxanthin on nonphotochemical quenching. NPQ kinetics calculated from chlorophyll fluorescence upon exposure of *N. gaditana* to different light/dark intervals. (*A*) NPQ activation measured with a 30-min treatment with saturating actinic light (800 µmol photons m^{-2} s^{-1}); data were fitted with a logistic function in red. (*B*) Repetition of two 8-min (8′) light treatments followed by 10 min′ dark relaxation. (*C*) Repetition of two 8-min light followed by 90 min′ dark. (*D*) Repetition of two 2-min light treatment followed by 10 min′ dark relaxation. Yellow and black boxes indicate light and dark intervals, respectively. In (*B–D*), the NPQ value reached after 30 s of light exposure both in the first and second light treatment was compared in the box plots on the right of each panel, and asterisks indicate statistically significant differences in NPQ activation between these two values (*t* test, *P*-value < 0.05). Data are expressed as average ± SD of three independent biological replicates.

Chlamydomonas reinhardtii and *Phaeodactylum tricornutum* to be essential for NPQ activation (6, 27).

When all strains above were cultivated in flasks at low density and optimal light (i.e., 100 µmol photons m^{-2} s^{-1}) for 4 d (*Material and Methods*), they showed no differences in growth with respect to the parental strain (*SI Appendix*, Fig. S4). Both *lhcx1* and *vde* KO strains showed a strong reduction of NPQ activation with respect to the WT (Fig. 3 *A* and *B*), while the *ZEP* OE strain instead showed a minor reduction in the NPQ activation capacity upon illumination, but also a faster relaxation when the light was switched off with respect to the parental strain (Fig. 3*C*).

In all strains, violaxanthin was the predominant xanthophyll (>80% VAZ), while antheraxanthin and zeaxanthin represent <10% and <5% of total VAZ content, respectively. Vaucheriaxanthin

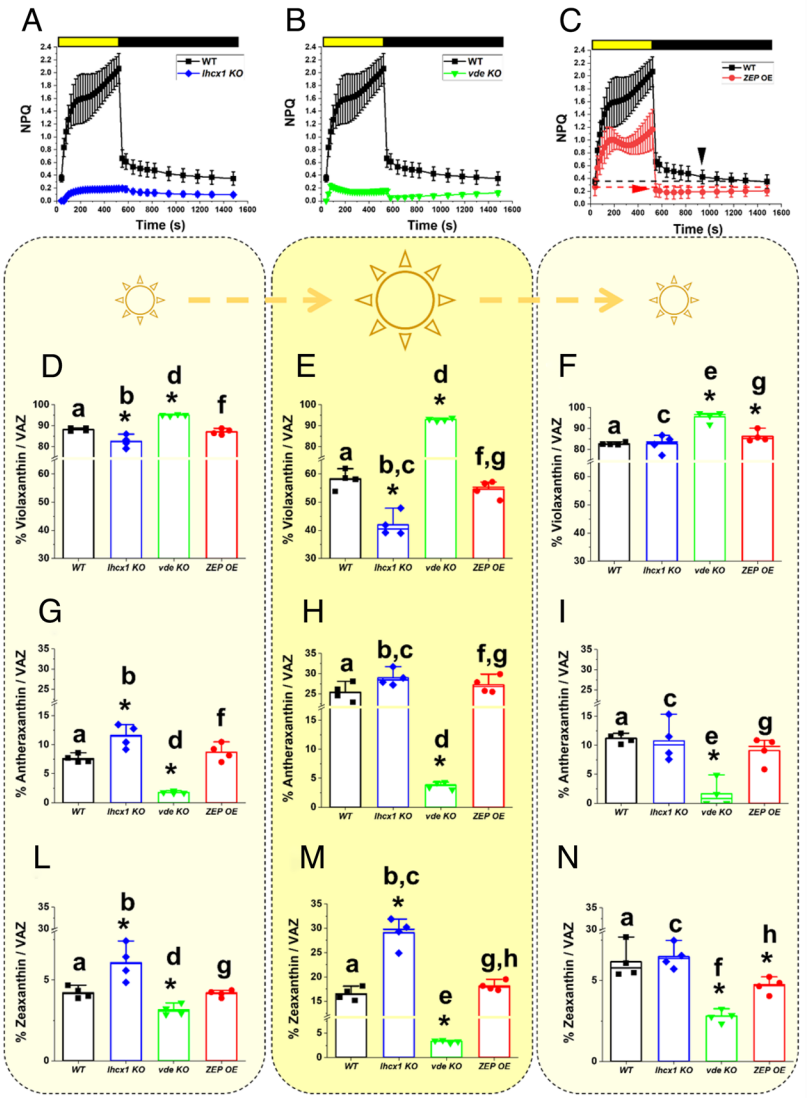

Fig. 3. Phenotypic characterization of *Nannochloropsis* strains with altered NPQ response and xanthophyll cycle. NPQ activation and relaxation kinetics for the WT *Nannochloropsis* strain (black squares) upon exposure to saturating light (yellow box) and dark (black box), respectively, compared to the *lhcx1 KO* (blue diamond, *A*), the *vde KO* (green downward triangle, *B*), and the ZEP-overexpressing strain (red circles, *C*). Cells were cultivated in flasks under optimal light (i.e., 100 µmol photons m^{-2} s^{-1}) for 4 d before NPQ evaluation. The two arrows in panel (*C*) indicate when the NPQ fully relaxes in the two strains. Xanthophyll content after cultivation for 4 d in liquid medium at optimal light (i.e., 100 µmol photons m^{-2} s^{-1}) (*D*, *G*, and *L*), upon treatment with saturating light (1,000 µmol photons m^{-2} s^{-1}) for 2 h (*E*, *H*, and *M*) and after recovery in optimal light for 1.5 h (*F*, *I*, and *N*) for the WT *Nannochloropsis* strain (black), the *lhcx1 KO* (blue), the *vde KO* (green), and the ZEP-overexpressing strain (red). Data are expressed as percentage of each xanthophyll molecule over their sum [violaxanthin, (*D*–*F*); antheraxanthin, (*G*–*I*); and zeaxanthin (*L*–*N*); VAZ]. Data are expressed as average ± SD of four independent biological replicates. Asterisks indicate statistically significant differences between each of the mutants and the parental strain, in every panel of the figure. Statistically significant differences in the content of each xanthophyll within the same strain, in different conditions (e.g., panels *D*–*F*), are indicated by the same alphabet letter (*t* test, *P*-value < 0.05).

and β-carotene were the other major carotenoids detected and they did not show any change in abundance either between genotypes or in the different light conditions tested (*SI Appendix*, Table S2), a result consistent with the hypothesis that the genetic modifications of these strains only affected the xanthophyll cycle.

While the *ZEP* OE did not show differences in the content of the three xanthophylls with respect to the parental strain, *lhcx1 KO* showed a reduction in the content of violaxanthin with a corresponding increase of both antheraxanthin and zeaxanthin (Fig. 3 *D*, *G*, and *I*), suggesting that the absence of the LHCX1 protein impacts the xanthophyll cycle as well. The *vde KO* strain showed instead an opposite trend, with an increased accumulation of violaxanthin and a corresponding reduction of the content of antheraxanthin and zeaxanthin with respect to the parental strain (Fig. 3 *D*, *G*, and *I*), suggesting that, in WT cells, VDE in this species has a minor activation even in the relatively low light used here during strain cultivation.

When treated with intense light (1,000 µmol photons m^{-2} s^{-1} for 2 h), *lhcx1* KO showed activation of the xanthophyll cycle but, interestingly, the accumulation of zeaxanthin and the corresponding decrease of violaxanthin were higher than those in the parental strain (Fig. 3 *E*, *H*, and *M*), suggesting that LHCX1 absence facilitates xanthophyll conversion upon excess light exposure. In *vde* KO, light treatment did not induce any significant change in antheraxanthin and zeaxanthin (Fig. 3 *D*, *G*, and *I*) and, as a result, upon saturating light, the content of violaxanthin was much larger in the *vde* KO than that in the WT (Fig. 3 *E*, *H*, and *M*). The *ZEP* OE instead did not show major differences in the accumulation of the three xanthophylls upon excess light exposure with respect to WT. This observation can be explained by the possibility that ZEP activity is inhibited under strong illumination by an unknown posttranslational mechanism. Alternatively, it is possible that *ZEP* overexpression was not strong enough to overcome endogenous VDE activity upon strong illumination, and thus it did not impact the overall balance of the xanthophyll composition upon prolonged exposure to saturating light (Fig. 3 *E*, *H*, and *M*).

After treatment with saturating light, all strains were then exposed again to optimal light for 1.5 h to monitor xanthophyll cycle relaxation. One and half hours was not enough to fully relax the xanthophyll cycle in the parental strain (Fig. 3 *F*, *I*, and *N*), as observed before (Figs. 1*D* and 2*C*). In the same time interval, *lhcx1 KO* was instead capable to restore the xanthophyll content measured before excess light exposure (Fig. 3 *F*, *I*, and *N*), demonstrating that the absence of LHCX1 facilitates xanthophyll conversion in both directions. In the same time, *ZEP* OE showed an increased accumulation of violaxanthin and a parallel reduction of zeaxanthin (24% lower with respect to WT) after 1.5 h recovery in optimal light, demonstrating that this

strain reconverted zeaxanthin into violaxanthin faster than the parental strain (Fig. 3*N*).

Impact of Xanthophyll Cycle on Photoprotection. All strains did not show any altered growth phenotype when cultivated on agar plates under optimal light (100 µmol photons m^{-2} s^{-1}, Fig. 4*A*). When exposed to strong, saturating illumination (500 µmol photons m^{-2} s^{-1}), the *vde* KO was the only strain showing a strong reduction in growth with respect to the parental strain (Fig. 4*B*), demonstrating a major role played by zeaxanthin in photoprotection.

To assess the impact of shorter light excess treatments, similar agar plates grown in optimal light (100 µmol photons m^{-2} s^{-1}) for 14 d were exposed to saturating light (1,000 µmol photons m^{-2} s^{-1}) for 2 h while monitoring photosystem II (PSII) quantum yield. All strains showed equal photosynthetic efficiency at the start of the experiment, after growth in optimal light conditions (Fig. 4*C*). Upon exposure to saturating light, there was a strong reduction of photosynthetic efficiency, because of multiple phenomena such as saturation of photosynthetic electron transport, NPQ activation, and damage to PSII. Both *lhcx1* and *vde* KO strains showed a smaller reduction than that of the WT (Fig. 4*C*), explainable by their inability to activate NPQ (Fig. 3), while the *ZEP* OE instead showed the same reduction observed in the WT (Fig. 4*C*).

While reoxidation of electron transporters and NPQ relaxation take a few minutes, PSII photoinhibition takes several hours to be recovered, and this different kinetics can be exploited to distinguish the different contribution to the decrease in photochemical yield observed in Fig. 4*C*. To this aim, cells were allowed to recover under dim light for 12 h, monitoring PSII quantum yield. After 4 h of recovery, *lhcx1 KO* showed a lower PSII quantum yield than that of the parental strain, suggesting that the mutation led to higher photoinhibition in this strain, although it recovered after 12 h of dim light. *vde KO* showed even larger differences, which were not fully recovered in the time monitored, suggesting that this strain had a larger photosensitivity with respect to the others (Fig. 4*C*).

The importance of both NPQ and the xanthophyll cycle to preserve photosynthetic functionality in oversaturating irradiances was confirmed by monitoring the photosynthetic activity of all strains upon treatment with increasing irradiances (*SI Appendix*, *Supporting Results* and Fig. S5). The *lhcx1 KO* and *vde KO* strains showed a faster decrease of qL (i.e., an estimation of photochemical capacity, *SI Appendix*, *Supporting Results*) as the light intensity increased, suggesting that their reaction centers were more easily saturated (*SI Appendix*, Fig. S5*C*), as well as a strong reduction of oxygen evolution upon exposure to increasing light (*SI Appendix*, Fig. S5*E*), highlighting the importance of NPQ and the xanthophyll cycle to preserve photosynthetic functionality in cells exposed to oversaturating irradiances. *ZEP* OE instead showed a slightly higher photochemical activity than that of the parental strain at saturating light intensities (*SI Appendix*, Fig. S5 *C* and *D*). *ZEP* OE also showed an increase of the photosynthetic electron transport (ETR) that also reached saturation at higher light intensities than that of the parental strain (*SI Appendix*, Fig. S5*B*).

Impact of Xanthophyll Cycle on Biomass Productivity in Photobioreactors. *Nannochloropsis* strains affected either in NPQ activation or xanthophyll cycle dynamics were cultivated in laboratory-scale photobioreactors to investigate the impact of photoprotection mechanisms on biomass productivity in industrially relevant conditions. In this setup, microalgae are cultivated in fed-batch mode at high biomass concentration (i.e., 1.5 g L^{-1}, 250 × 10^6 cells mL^{-1}). Because of the high optical density, the first layers of the cultures are fully exposed to illumination, while cells deeper in the volume are in light limitation (28). Environmental complexity is further increased by the culture mixing, causing cells to abruptly move from limiting illumination to full irradiation and vice versa.

Cultures were exposed to two irradiances, namely 400 and 1,200 µmol photons m^{-2} s^{-1}, as depicted in *SI Appendix*, Fig. S6. Both irradiances are saturating for *Nannochloropsis*, well beyond the saturation limit of 150 µmol photons m^{-2} s^{-1} (19), and cells exposed to these illumination intensities thus experience light excess and activate the xanthophyll cycle. Because of the culture optical density, however, most of the cells deeper in the culture [approx. >1 and >2 cm out of 5 total cm for an incident illumination of 400 and 1,200 µmol photons m^{-2} s^{-1}, respectively (28)] were still light limited. Overall, this setup was chosen to reproduce the complex light environment experienced by microalgae during outdoor industrial cultivation in the laboratory, where cells most exposed to illumination experience light excess, while deeper layers are under light limitation. Cultures were diluted

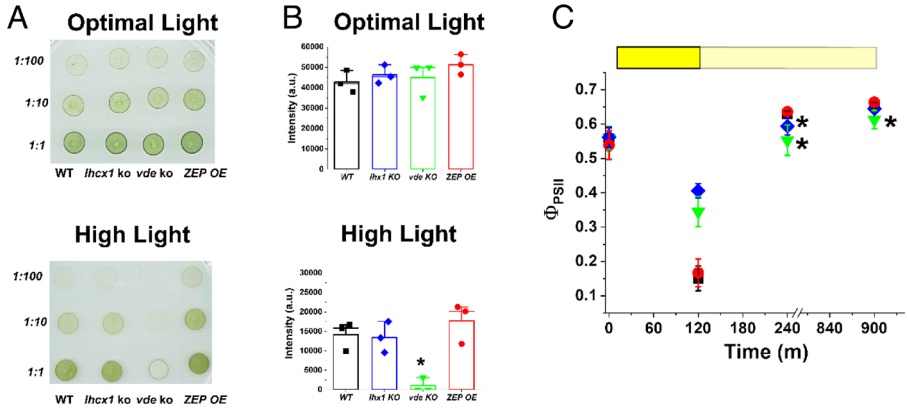

Fig. 4. Impact of the xanthophyll cycle on photoprotection. (*A*) Agar plates with spots starting from the same cell concentration (i.e., 9 × 10^6 cells mL^{-1} for the 1:1 dilution) for all the strains with different degrees of alteration of the xanthophyll cycle used in this work. Plates were supplemented with 10 mM $NaHCO_3$ to avoid carbon limitation and they were grown for 14 d at 100 and 500 µmol photons m^{-2} s^{-1}, respectively, for optimal and high light conditions. Strain ID is indicated on the bottom, while dilution factor is on the left. (*B*) Quantification of the intensity of the spots was performed with the software ImageJ (v. 1.52; https://imagej.nih.gov/ij/index.html) and it is here presented for the 1:10 dilution of the plates reported in panel *A*. The asterisk indicates statistically significant difference between the *vde KO* and the parental strain (*t* test, *P*-value < 0.05). (*C*) Photosynthetic efficiency of all the strains used in this work after treatment with saturating light (1,000 µmol photons m^{-2} s^{-1}) for 2 h (yellow box) and upon recovery in dim light (pale yellow box) for 12 h. WT *Nannochloropsis* strain, black squares; *lhcx1 KO*, blue diamonds; *vde KO*, green downward triangles; ZEP-overexpressing strain, red circles. Data are expressed as average ± SD of three independent biological replicates. Asterisks indicate statistically significant differences between each of the mutants and the parental strain at a specific time point (*t* test, *P*-value < 0.05).

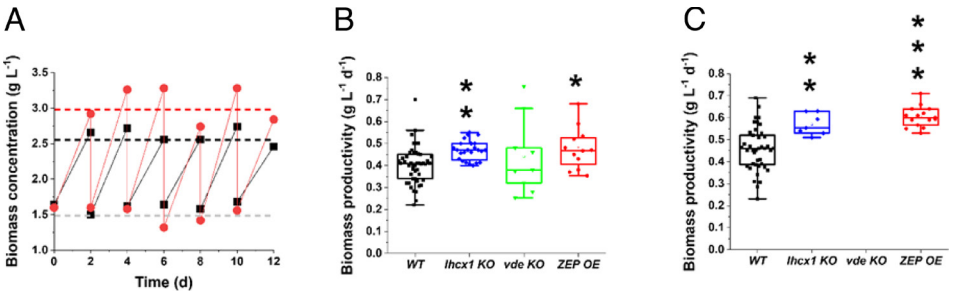

Fig. 5. Biomass productivity of *Nannochloropsis* semi-continuous cultures. (*A*) Operational scheme for *Nannochloropsis* semi-continuous cultures. Data were collected before and after dilution to restore the initial biomass concentration of 1.5 g L^{-1}, for both WT (black squares) and ZEP overexpressor (red circles). This panel shows a small timeframe of much longer sampling campaigns. Biomass productivity of *N. gaditana* strains investigated in this work, upon exposure to 400 (*B*) and 1,200 µmol photons m^{-2} s^{-1}. (*C*) Asterisks indicate statistically significant differences between each of the different strains and the WT in the same panel (*t* test, **P*-value < 0.05; ***P*-value < 0.01; ****P*-value < 0.001). All strains show a greater biomass productivity at 1,200 than that at 400 µmol photons m^{-2} s^{-1} (*t* test, *P*-value < 0.01); n > 10 and in some cases, the number of samples was larger than 30. Part of the semi-continuous data used to calculate biomass productivity values in *B* and *C* are reported in *SI Appendix*, Fig. S7.

every other day to restore the initial biomass concentration (*SI Appendix*, Fig. S7), and biomass concentration before and after dilution was used to calculate biomass productivity for all the strains investigated (Fig. 5*A*).

When exposed to higher irradiance, we observed a reduction in Chl and an increase in carotenoids (Car) content for all the strains investigated in this work, indicating activation of an acclimation response (29), but without showing major differences between strains (*SI Appendix*, Table S3).

Maximal photosynthetic efficiency (Φ_{PSII}) showed a general reduction upon cultivation at stronger irradiance, likely because of some photoinhibition. Maximal photosynthetic efficiency did not show major differences between the strains here investigated, with the exception of *vde* KO (*SI Appendix*, Table S4).

With 400 µmol photons m^{-2} s^{-1} illumination, *lhcx1* KO and *ZEP* OE showed a higher biomass productivity than that of the WT, while no difference was observed for *vde* KO (Fig. 5*B*).

The improved growth of the ZEP OE strain was confirmed also in other two independent overexpression lines (*SI Appendix*, Fig. S8*A*) generated in this work (*SI Appendix*, Fig. S3). The stability of the overexpression of the *ZEP* gene, as well as the increased accumulation of the ZEP protein, was validated via qRT-PCR (*SI Appendix*, Fig. S8*B*) and mass spectrometry (*SI Appendix*, Fig. S9), respectively, in all three genetic lines during biomass productivity tests, demonstrating that this indeed represents the molecular basis of the productivity advantage here observed.

When irradiance increases up to 1,200 µmol photons m^{-2} s^{-1}, all cultures produced more biomass and the difference between the *ZEP* OE and *lhcx1* KO with respect to the parental strain increased, while the *vde KO* did not survive (Fig. 5*C*). As shown in *SI Appendix*, Fig. S10, *vde KO* was unable to maintain sufficient cell duplication rate and maintain the cell concentration of the culture upon exposure to strong illumination.

In order to confirm the highly different impact of LHCX1 and VDE absence on biomass productivity, analogous mutants impaired in NPQ activation and zeaxanthin biosynthesis (i.e., *lhcx1 KO* and *vde KO*, respectively) from another species of the same genus, *N. oceanica*, were similarly analyzed (30). Also in this case, the *vde KO* strain showed strong sensitivity to high light exposure (*SI Appendix*, Fig. S10*C*), while *lhcx1 KO* was fully able to survive high irradiance in dense cultures and showed higher biomass productivity than that of the WT in these conditions (*SI Appendix*, Fig. S10*B*). This confirms that the strong sensitivity of the *vde KO* strain was due to the biological role of zeaxanthin in acclimating to saturating irradiances in *Nannochloropsis*, with a strong impact that was evident even in two different species.

Impact of Xanthophyll Cycle Dynamics on the Response to Light Fluctuations. One major feature of dense cultures in photobioreactors is that microalgae are exposed to inhomogeneous irradiance, and they can suddenly move from excess to limiting light conditions and vice versa. To assess the impact of xanthophyll cycle on response to dynamic light regimes in more detail, we simulated the fluctuations of irradiance cells' experience in dense cultures and measured the impact on photosynthetic activity, quantified from oxygen evolution using a high-sensitivity instrumentation (Fig. 6). Light fluctuations were designed to provide, on average, an optimal number of photons for *Nannochloropsis* [i.e., 100 µmol photons m^{-2} s^{-1}, (26)] but through cycles of saturating and limiting illumination (i.e., 300 and 15 µmol photons m^{-2} s^{-1}, respectively) for different time frames (i.e., 3 and 7 min, respectively) in order to highlight any eventual difference in response to strong illumination or limiting light (Fig. 6*A*).

O_2 evolution in WT cells changed following the light irradiance dynamics, as expected (Fig. 6*A* and *SI Appendix*, Table S5). Cells were first exposed to a constant optimal light intensity at 100 µmol photons m^{-2} s^{-1} to reach a steady photosynthetic activity (9.3 ± 1.4 pmol O_2 s^{-1} 10^{-6} cells). When light increased to 300 µmol photons m^{-2} s^{-1}, photosynthetic activity followed, reaching a new steady state after approx. 2 min (12.45 ± 4.5 pmol O_2 s^{-1} 10^{-6} cells). When light decreased to 15 µmol photons m^{-2} s^{-1}, photosynthetic activity decreased to reach a lower steady oxygen evolution rate after approx. 4 min (1.31 ± 0.17 pmol O_2 s^{-1} 10^{-6} cells, *SI Appendix*, Table S5).

The same light fluctuation was then repeated eight times covering a total of 80 min, followed by another exposure at optimal constant light at 100 µmol photons m^{-2} s^{-1} (Fig. 6*B*). The repetition of light fluctuations had a clear effect on *Nannochloropsis* photosynthetic activity. The oxygen evolution activity of the WT at steady 100 µmol photons m^{-2} s^{-1} illumination after the fluctuation treatment was significantly reduced to 5.8 ± 0.8 pmol O_2 s^{-1} 10^{-6} cells, which is 37% lower than before (Fig. 6*B*). Consistently, the trace in Fig. 6*B* suggested that also oxygen evolution activities at 300 and 15 µmol photons m^{-2} s^{-1} progressively decreased with each fluctuation cycle, as confirmed when these trends were analyzed in detail, showing a significant linear decay (Fig. 6 *C* and *D*, respectively). Clearly, these data suggest that light fluctuations caused a decrease in photosynthetic activity, because of the activation of photoregulatory mechanisms and photoinhibition.

The reduction of photosynthetic rates observed at 15 µmol photons m^{-2} s^{-1} is relatively larger than the one observed at 300 µmol photons

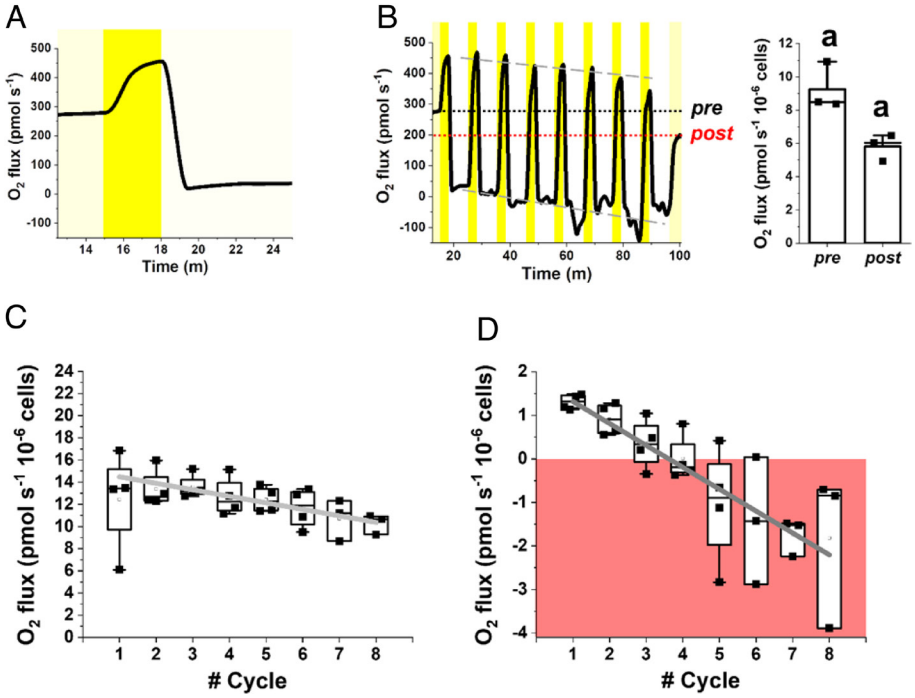

Fig. 6. Photosynthetic functionality of WT *Nannochloropsis* in fluctuating light. Oxygen evolution of the WT *Nannochloropsis* strain was measured in 2 mL samples at a concentration of 100 × 10^6 cells mL^{-1} (see *Materials and Methods* for details). (*A*) We designed a method to treat cells with a light fluctuation protocol where they were first exposed to optimal light at 100 µmol photons m^{-2} s^{-1} (yellow box) until a steady photosynthetic activity was reached, then to 300 µmol photons m^{-2} s^{-1} (dark yellow box) and 15 µmol photons m^{-2} s^{-1} (light yellow box) for 3 and 7 min, respectively. Irradiance and time of exposure were set so as to provide cells with an optimal number of photons, corresponding to 100 µmol photons m^{-2} s^{-1}. (*B*) The two phases at 300 and 15 µmol photons m^{-2} s^{-1} were repeated eight times and after cells were returned to an optimal irradiance of 100 µmol photons m^{-2} s^{-1}. Black and red dot lines indicate the oxygen flux at 100 µmol photons m^{-2} s^{-1} before (pre) and after (post) light fluctuation, respectively. Gray dashed lines instead indicate the trend of oxygen flux over the fluctuation cycles. The oxygen evolution activity pre- and post-light fluctuation was compared to measure the impact of light fluctuation on photosynthetic activity (right plot in panel *B*). The same alphabet letter indicates statistically significant differences between oxygen evolution values at 100 µmol photons m^{-2} s^{-1}, before and after light fluctuation (*t* test, *P*-value < 0.05). Oxygen evolution activity of WT cells at 300 µmol photons m^{-2} s^{-1} (*C*) and 15 µmol photons m^{-2} s^{-1} (*D*) over the number of fluctuation cycles. Data at a specific light intensity come from the average oxygen evolution rate measured over 20 s of the trace in *A*. In *D*, the area where oxygen consumption via respiration is higher than oxygen evolved via photosynthesis is highlighted by a red box. At both irradiances, photosynthetic activity significantly drops (slope is significantly different from zero, *t* test, *P*-value < 0.05) over the fluctuation cycles, according to the following linear functions: y = (15.07 ± 0.35) – (0.59 ± 0.06) x, Pearson's R: −0.97, R-Square: 0.94 (*C*); y = (1.82 ± 0.045) – (0.5 ± 0.01) x, Pearson's R: −0.99, R-Square: 0.99. (*D*) Data are expressed as average ± SD of four independent biological replicates.

m^{-2} s^{-1} (Fig. 6 *D* and *C*, respectively). Even more importantly, at low illumination, the activity became negative, meaning that in these cells, photosynthesis is not able to compensate for respiration (Fig. 6*D*). These data are particularly informative on the behavior of microalgae cells in dense cultures of industrial systems, where cells are exposed to continuous light fluctuations and a large fraction of the culture volume is light limited (18), and suggest that these cells might indeed have negative photosynthetic activity, thus curbing overall photon-to-biomass conversion efficiency and biomass productivity.

The strains affected in photoprotection and the xanthophyll cycle were also exposed to the same light profile. At 100 µmol photons m^{-2} s^{-1} constant illumination, *vde KO* and *ZEP OE* showed the same photosynthetic activity of the WT, while *lhcx1 KO* instead showed a significant reduction (*SI Appendix*, Table S5). After exposure to light fluctuations, *vde KO* showed a significant reduction of photosynthetic activity at 100 µmol photons m^{-2} s^{-1} (32%), similar to WT. On the contrary, the photosynthetic activities of both *lhcx1 KO* and *ZEP OE* were not affected (Fig. 7 *A*, *E*, and *I*). The WT strain activated NPQ during the 3 min of excess light exposure and this effect was additive over the course of the light fluctuation protocol (Fig. 7*C*), because of the contribution of the preexisting zeaxanthin, as already observed in Fig. 2. *Lhcx1 KO* did not show any NPQ activation during light fluctuation, as expected (Fig. 7*C*) but also it did not show any sign of photodamage after the treatment since there was a complete recovery of PSII quantum yield after 30 min (Fig. 7*D*). This phenotype of *lhcx1 KO* suggests that the reduction of oxygen evolution activity upon exposure to light fluctuations observed in the WT was largely due to NPQ activation rather than PSII damage.

The *ZEP OE* strain also activated NPQ upon exposure to strong light, but at a lower intensity than the WT, as previously observed in Fig. 3*C*. The cumulative effect of zeaxanthin on NPQ was lost in this strain, likely because of the faster reconversion of zeaxanthin into violaxanthin during the low light phases (Fig. 7*M*). *ZEP OE* did not show any sign of photosensitivity under the same conditions (Fig. 7*N*), suggesting that cells were still capable of withstanding light fluctuations.

Vde KO also did not show NPQ activation during light fluctuations, as expected (Fig. 7*G*). The decrease of PSII quantum yield at the end of the treatment indicated photodamage, confirming a higher photosensitivity of the strain (Fig. 7*H*).

All mutant strains showed a significant reduction of the oxygen evolution activity at 15 µmol photons m^{-2} s^{-1} over the cycles of fluctuations, as observed in the WT (Fig. 7 *B*, *F*, and *I* and *SI Appendix*, Table S6). Both *lhcx1 KO* and *ZEP OE* showed a smaller reduction over the cycles of fluctuations and oxygen evolution activity at 15 µmol photons m^{-2} s^{-1} became negative after five cycles, different from WT and *vde KO* where negative values were reached only after three cycles of fluctuation (Fig. 7 *B*, *F*, and *I*). After the treatment, oxygen evolution at 15 µmol photons m^{-2} s^{-1} was −0.44 ± 0.37 pmol O_2 s^{-1} 10^{-6} cells for *lhcx1 KO* and −0.95 ± 1.35 pmol O_2 s^{-1} 10^{-6} cells for *ZEP OE*, while −1.81 ± 1.7 pmol O_2 s^{-1} 10^{-6} cells for WT and −2.9 ± 0.9 pmol O_2 s^{-1} 10^{-6} cells for *vde KO* (Fig. 7).

Discussion

Biological Role of Zeaxanthin in *Nannochloropsis*. *Nannochloropsis gaditana* cells upon exposure to excess light show the ability to convert violaxanthin into zeaxanthin (Fig. 1), as in many other photosynthetic eukaryotes (17). *Nannochloropsis* has a peculiar pigment composition, with violaxanthin being the most abundant carotenoid in this species, accounting for approx. 50% of the total (31–33). Likely because of this large reservoir of substrate, in contrast to plants and other microalgae (34, 35), zeaxanthin synthesis in *Nannochloropsis* continues even upon prolonged exposure to extreme irradiances with no visible saturation (Fig. 1). Considering the light intensities tested in this work, which went well beyond physiologically relevant conditions, our results also suggest that zeaxanthin synthesis is unlikely to ever reach saturation in the natural environment, meaning that *Nannochloropsis* cells are capable of additional zeaxanthin synthesis whenever needed even if they have already been exposed to strong illumination.

The large capacity of zeaxanthin synthesis is accompanied by a strong impact of this pigment on the protection of the photosynthetic apparatus. The phenotype of both *vde* KO and WT cells treated with the VDE inhibitor DTT demonstrates that zeaxanthin synthesis has a major impact on NPQ in *Nannochloropsis* (Fig. 3*B* and *SI Appendix*, Fig. S1), as also observed in ref. 30.

Zeaxanthin synthesis impacts NPQ from the first few seconds of illumination (Fig. 2), while HPLC analysis shows that a few minutes of illumination are needed before detecting a significant accumulation of molecules (Fig. 1). This observation suggests that a small number of zeaxanthin molecules can activate NPQ in a few seconds after an increase of illumination, likely by associating to specific binding sites in light-harvesting complexes. Considering that also *lhcx1* KO strain shows a major decrease in NPQ capacity, and that its full activation requires the presence of both zeaxanthin and LHCX1, it is likely that zeaxanthin activity in NPQ requires its association to the LHCX1 protein in *N. gaditana*, as previously suggested for *N. oceanica* (30). Similarly, in diatoms, NPQ is

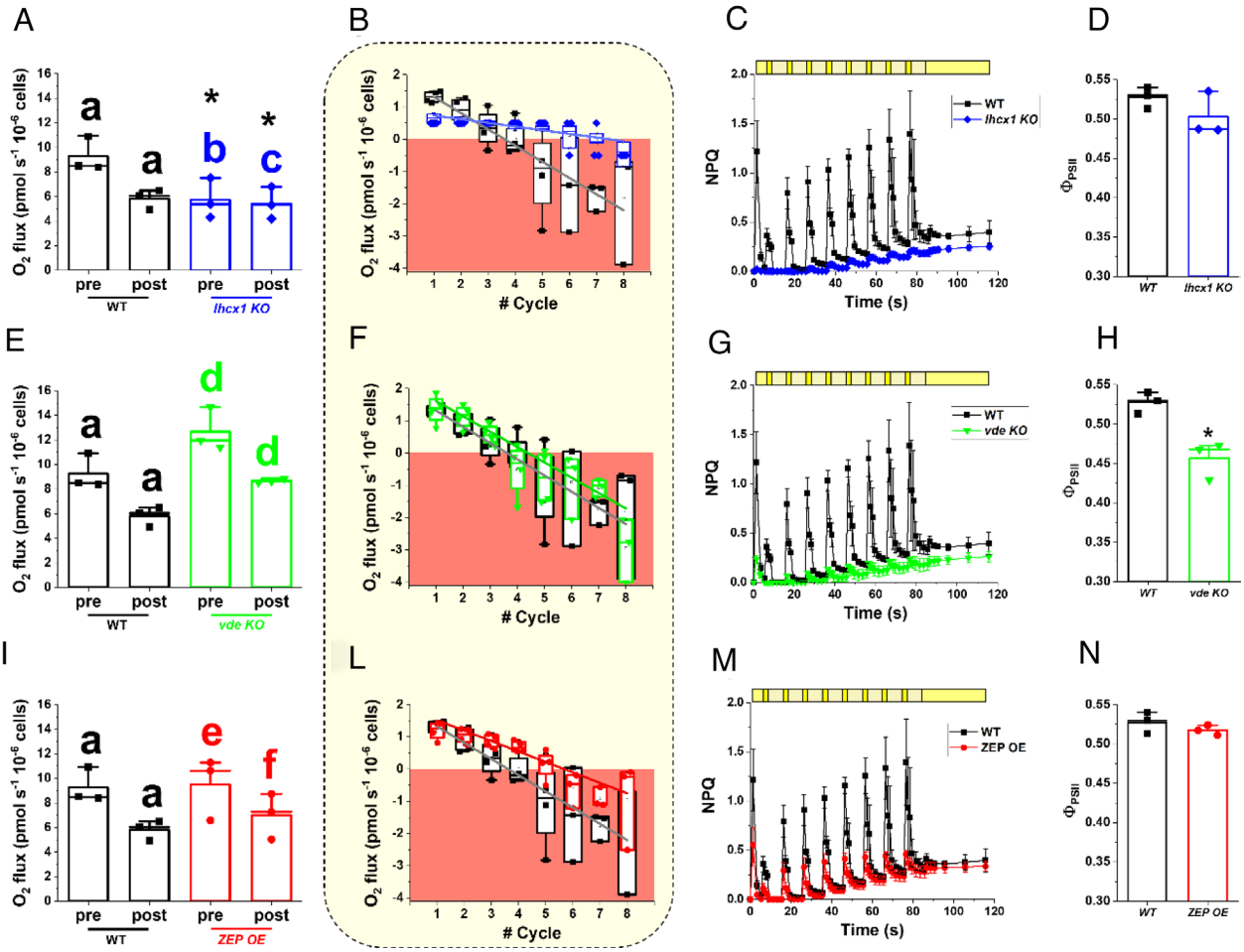

Fig. 7. Photosynthetic functionality of strains affected in NPQ and xanthophylls cycle dynamics in fluctuating light. Photosynthetic functionality is expressed as oxygen evolution activity and was measured in the conditions described in Fig. 6. Oxygen evolution activity of *lhcx1 KO* (*A*), *vde KO* (*E*), and *ZEP OE* (*I*) before (pre) and after (post) the light fluctuation treatment of Fig. 6, compared to the WT. Data are expressed as average ± SD of three independent biological replicates. The same alphabet letter indicates statistically significant differences between oxygen evolution values at 100 µmol photons m^{-2} s^{-1}, before and after light fluctuation within the same strain, while asterisks indicate statistically significant differences between mutants and WT (*t* test, *P*-value < 0.05). Oxygen evolution activity for *lhcx1 KO* (blue diamonds, *B*), *vde KO* (green downward triangles, *F*) and *ZEP OE* (red circles, *L*) cells at 15 µmol photons m^{-2} s^{-1} (light yellow box) over the number of fluctuation cycles compared to the WT (black squares). The area where oxygen consumption via respiration is higher than oxygen evolved via photosynthesis is highlighted by a red box. The linear oxygen evolution trend over the cycles of fluctuation has been mathematically described by the functions reported in *SI Appendix*, Table S6. Data are expressed as average ± SD of four independent biological replicates. NPQ kinetics upon exposure to light fluctuation in the *lhcx1 KO* (blue diamonds, *C*), *vde KO* (green downward triangles, *G*), and *ZEP OE* (red circles, *M*) cells compared to the WT (black squares). Yellow boxes indicate the light regime followed during light fluctuation, as previously described in Fig. 6. The final light treatment at 100 µmol photons m^{-2} s^{-1} was increased to 30 min to give the WT strain enough time to recover photosynthetic functionality. Afterward, a final saturating pulse was used to measure the photosynthetic efficiency and assess photoinhibition because of the light fluctuation (*D*, *H*, and *N*, respectively for *lhcx1 KO, vde KO,* and *ZEP OE*). In both NPQ and photoinhibition panels, data indicate the average ± SD of three independent biological replicates. The asterisk indicates statistically significant difference between the *vde KO* strain and the WT (*t* test, *P*-value < 0.05).

provided by a concerted action between LHCX proteins and diatoxanthin (36), a xanthophyll molecule part of the diadinoxanthin–diatoxanthin cycle, which is analogous to the VAZ cycle observed in *Nannochloropsis* (37). LHCX1 is the main NPQ effector also in diatoms, although additional LHCX proteins, namely LHCX2 and LHCX3, are involved when cells are exposed to prolonged high light, providing flexibility of quenching site but most likely with a similar mechanism (36, 38, 39).

Pigment data of the *lhcx1 KO* strain also show that the absence of LHCX1 has a measurable impact on the xanthophyll cycle dynamics with a larger accumulation of zeaxanthin than that in WT, but also a faster conversion back to violaxanthin. This can be explained knowing that a large fraction of violaxanthin is bound to antenna proteins and it needs to be released into the thylakoid membrane to be converted into zeaxanthin. This exchange from antenna proteins limits the rate of xanthophyll conversion, as demonstrated in plants (40). *lhcx1 KO* is depleted of one of the most abundant antenna proteins in *Nannochloropsis* (41), and this is likely to accelerate zeaxanthin synthesis and degradation because of a larger presence of carotenoids not bound to antenna proteins, but free in the thylakoid membranes and thus more available to VDE.

In *N. gaditana*, even though NPQ slowly continues to increase after 10 min induction, suggesting the presence of a qZ-type contribution associated with the progressive accumulation of zeaxanthin, the largest fraction of NPQ capacity reaches saturation in this time frame (Fig. 2). Since zeaxanthin synthesis continues much longer without showing signs of saturation (Fig. 1), this suggests that the influence of zeaxanthin molecules on NPQ reaches saturation, likely because of saturation of the potential binding sites for zeaxanthin in LHCX1. A second, larger, pool of zeaxanthin molecules continues to be synthesized upon prolonged exposure to strong light, but it does not contribute to NPQ and likely plays other roles in photoprotection such as direct scavenging of Chl triplets and ROS (9).

While the zeaxanthin molecules active in NPQ are quickly synthesized, their impact on NPQ remains for a prolonged time. This is evidenced by the fact that NPQ induction kinetics are faster if cells have already been exposed to a previous light treatment (Fig. 2). This effect is already visible after exposing cells to light for 2 min and it is still detectable after a 90-min dark relaxation, demonstrating that this time is not sufficient to reconvert all zeaxanthin synthesized in 8 min illumination (Fig. 2). This effect can be modulated by overexpressing ZEP since cells are faster in reconverting zeaxanthin into violaxanthin during the 90-min dark relaxation, as demonstrated by the reduction in NPQ induction during the second kinetic with respect to the parental strain (*SI Appendix*, Fig. S11), supporting the HPLC data of Fig. 3.

Zeaxanthin Plays an Essential Photoprotective Role in *Nannochloropsis*, beyond NPQ. Both *vde KO* and *lhxc1* KO strains show sensitivity to saturating illumination, supporting the role of NPQ on protection of *Nannochloropsis* from light stress (Fig. 4). When cells are cultivated in dense cultures, however, the results between the two genotypes are very different. In this context, some cells are exposed to full illumination, while the others, because of shading, are in limiting light or even dark (28). In the experimental system employed here, approx. 60% of incident radiation is absorbed by the 1st cm of culture depth (18). If the culture is exposed to a strong external illumination (1,200 µmol photons m^{-2} s^{-1}), *vde* KO cells show a clear decrease in maximum quantum yield of PSII (*SI Appendix*, Table S4), suggesting that more exposed cells are extensively damaged by illumination. This damage cannot even be counterbalanced by cells deeper in the culture volume and eventually it impairs the growth of the whole culture under strong illumination (*SI Appendix*, Fig. S10).

The inability of the *vde* KO strain to grow at higher illumination depends on its stronger photosensitivity as a consequence of the absence of both the NPQ response and the activation of the xanthophyll cycle upon exposure to saturating irradiance, as demonstrated in Figs. 3–5. While *vde KO* and *lhcx1* KO strains are similarly defective in NPQ (Fig. 3), the latter retains ability to growth under strong illumination in very different conditions, such as agar plates (Fig. 4) and laboratory-scale photobioreactors (Fig. 5), while *vde KO* shows strong impairment in both. Moreover, the *lhcx1 KO* in those conditions does not show any additional photodamage with respect to WT (Fig. 4), clearly demonstrating that the impact of zeaxanthin biosynthesis on photoprotection goes well beyond its role in enhancing NPQ and that its ability to increase scavenging of Chl triplets and ROS (9, 42) is essential even in dense cultures.

Xanthophyll Cycle Dynamics Has a Major Impact on Microalgae Biomass Productivity in Photobioreactor. Microalgae at industrial scale are cultivated at high concentration to maximize biomass productivity. Such dense cultures are also continuously mixed to maximize the exposure of cells to incident light and avoid nutrient and carbon limitation, causing cells to suddenly move between limiting and excess illumination, further increasing the complexity of the light environment. In these environmental conditions, more exposed cells need photoprotection mechanisms to withstand strong illumination, but the same mechanisms become detrimental for productivity once the cells move to light limitation of deeper layers. The trade-off between photoprotection and photochemical efficiency, which must be balanced by all photosynthetic organisms (3), is thus particularly challenging in such a complex and dynamic environmental context. It is not surprising that strategies for the optimization of photosynthetic productivity have generated mixed results so far (43, 44), with the only reasonable conclusion being that the complexity of the natural and artificial changes experienced by microalgae during industrial cultivation has a major influence on productivity that cannot be underestimated (45).

Strains with altered xanthophyll cycle analyzed in this work demonstrate that an efficient photoprotection is essential for microalgae fitness in dense cultures to ensure growth under full sunlight, as shown by the strong photosensitivity of *vde* KO. On the contrary, we observed that *lhxc1* KO in dense cultures shows a positive impact on biomass productivity. This strain differs from WT not only because of its reduction in NPQ activation, but also for a reduced PSII antenna size and Chl content per cell (46) and a higher zeaxanthin content, observed in this work. Mathematical models suggest that the reduction in Chl content per cell should have the largest impact in improving biomass productivity (46), but it is also possible that the higher zeaxanthin content observed in *lhcx1* KO can be beneficial to compensate for any eventual extra damage due to NPQ inactivation. Overall, this work demonstrates that an indiscriminate reduction of photoprotection mechanisms is detrimental for growth even in dense cultures typical of industrial cultivation systems. In fact, cells most exposed to illumination experience light saturation and eventually damage. While the zeaxanthin impact on photoprotection is clear, the impact of NPQ is more complex. The *lhcx1 KO* strain is impaired in NPQ but also has a reduction of both Chl content/cell and PSII antenna size (ASII) that are beneficial for cultivation in dense cultures. Overall, these results confirm that the reduction of NPQ alone has a limited impact on biomass productivity in dense microalgae cultures, at least in *Nannochloropsis* (46, 47).

Energy losses due to natural kinetics of photoprotection can however be detrimental for productivity in low light conditions, and accelerating zeaxanthin conversion to violaxanthin can be advantageous in this context. The impact on the overall xanthophylls pool that we observed because of the overaccumulation of the ZEP protein was quite modest and when we measured the relaxation kinetic at earlier time points (i.e., 5, 10, and 15 min of recovery in the dark), the differences between the *ZEP OE* and the WT strains were even smaller (*SI Appendix*, Fig. S12). On the contrary, also these data highlight a difference in the biological role of zeaxanthin, depending on its binding localization, with a relatively small pool hypothetically binding LHCX1 and involved in NPQ activation/relaxation. The overexpression of ZEP likely shows a much stronger effect on this latter pool of zeaxanthin with the largest impact on NPQ, explaining why differences are observable by measuring NPQ kinetics, but they are too small to be assessable by HPLC.

In this work, we also simulated the light fluctuation experienced by microalgae in dense cultures of industrial systems (Fig. 6*B*) as a consequence of mixing and observed that WT cells showed a substantial reduction of photosynthetic functionality in light limitation after only a few fluctuation cycles (Fig. 6*D*). This decrease could be due to multiple phenomena, such as the activation of photoprotection or photoinhibition. The *lhcx1 KO* strain does not show the same reduction of WT, suggesting that NPQ is the major factor responsible for the loss of activity observed in the parental strain in dense cultures. On the contrary, the *vde KO* strain showed an even larger reduction of photosynthetic functionality in light limitation (Fig. 7*F*), suggesting that photoinhibition can also play a major role, as measured in Fig. 7*H*.

In the case of the *ZEP* OE, cells maintain the ability to activate NPQ but also have faster recovery, suggesting that increasing the rate of violaxanthin biosynthesis alone has a beneficial effect on productivity. This is achieved because cells have a faster reconversion rate to violaxanthin when light becomes limiting, which likely provides an advantage when cells move from external to internal, light-limited positions in the dense culture, where they remove zeaxanthin faster and can therefore channel more energy toward photochemistry. These properties, however, also represent a potential cost, in terms of lower photoprotection, when cells move in the opposite direction from internal to external layers. This cost, however, is lower than the advantage, because of two main reasons. One is that the cells still maintain the ability to synthesize zeaxanthin when needed for photoprotection (Fig. 3) and two, in all tests run here, there were no major signs of increased damage.

It is also worth noting that light-limited layers represent the major fraction of the volume in dense cultures of industrial systems (an estimated >70% of the culture volume for the setup schematized in *SI Appendix*, Fig. S6*A*) (18), and therefore it can be expected that a large fraction of the culture benefits from this genetic optimization, while there is a smaller fraction that might eventually have a modest disadvantage. Consequently, even a modest increase in the speed of reconversion of zeaxanthin into violaxanthin can provide a substantial effect on biomass productivity. This is consistent with the observation that *lhcx1 KO* and *ZEP* OE, the two strains that show the smaller reduction in photosynthetic activity upon exposure to light fluctuations, also showed an increase in biomass productivity in dense cultures (Fig. 5). This suggests that the optimization of the xanthophyll cycle is a valuable strategy in photosynthesis engineering, yet a fine-tuning is preferable to an indiscriminate activation, likely because in the latter case, the improvement in cell fitness cannot fully compensate the metabolic burden of a hyperactive xanthophyll cycle.

Optimization of Xanthophyll Dynamics in Microalgae vs. Plants. The genetic modification of NPQ and xanthophyll cycle has already been demonstrated to be effective to improve biomass productivity in crop plants in the field (14, 15). In our current work, effects are observed in *Nannochloropsis* by overexpressing only ZEP. It is in fact worth mentioning that VDE activity remains strong in the *ZEP* OE strain, such that it is still fully capable of producing zeaxanthin upon excess light exposure. This is likely also connected with a high violaxanthin content of *N. gaditana* with respect to plants, suggesting that this organism likely also has high endogenous VDE activity.

However, when metabolic engineering is applied to photosynthesis, the complexity of the environmental conditions of the intended cultivation system should also be considered, as well as the physiology of the species targeted for improvement. For instance, in plants of *Nicotiana benthamiana*, *Arabidopsis thaliana,* and *Solanum tuberosum*, VDE, ZEP, and PSBS overexpression did not show the same effects (48, 49), indicating that species-specific physiological or morphological features are highly influential on the homeostasis of the photosynthetic metabolism.

In the environment of photobioreactors, most of the culture is light limited, while only a small layer of cells is exposed to full sunlight. The design of photobioreactors, as well as operational conditions (e.g., culture concentration), strongly affects the percentage of cells that are in light-limiting conditions or excess light, affecting the optimal balance between photoprotection and photochemical efficiency. Culture mixing is also expected to play a major role on this balance. It is then worth noting that the complexity of the natural and artificial changes experienced by microalgae in dense cultures of industrial systems is likely to prevent the identification of ideal strains more productive in all operational conditions, suggesting that photosynthesis optimization efforts should be tuned to the specific operational conditions in use.

Materials and Methods

Isolation of *vde KO* Strain in *Nannochloropsis*. *Nannochloropsis vde KO* mutant strain was isolated via homology-directed repair mediated by CRISPR-Cpf1 technology, using recombinant ribonucleoproteins (RNPs). The construct to drive homology repair was designed to contain a cassette conferring resistance to Zeocin (50), flanked on both sides by 1.5 kb genomic regions homologous to the 5′ and 3′ of the *VDE* gene of *Nannochloropsis* (Gene ID: rna9604). The homology repair cassette was then excised from the holding vector and used to transform *Nannochloropsis* according to ref. 50. Prior to transformation, 4 µL of three synthetic RNPs, assembled using recombinant Cpf1 and synthetic sgRNAs (IDT Technologies) in an equimolar ratio (6 µM), at RT for 20 min, were added to the sample to drive three independent events of site-directed double-strand cleavage in the *VDE* gene. sgRNA sequences used in this work from 5′ to 3′ were 1. gaccaccgcgcgggtgacggcgg; 2. cgtgcagggcgaccggctctacg; and 3. gcgaggtcgccgggtttctggtt.

Strains, Cultivation Conditions, and Growth Monitoring.

Strains. In this work, we used two species: *N. gaditana* and *Nannochloropsis oceanica*. All strains used in this work are summarized in Table 1.

N. gaditana, strain CCAP 849/5, was purchased from the Culture Collection of Algae and Protozoa (CCAP). *N. gaditana lhcx1 KO* was previously obtained by insertional mutagenesis (26, 50). *N. gaditana* strains *vde KO* and the *ZEP* overexpressor were generated in this work, the former via CRISPR-Cpf1, while the latter after transformation with a cassette conferring resistance to Zeocin (50) flanking another one expressing the coding sequence of the endogenous *ZEP* gene (Gene ID: rna3613).

N. oceanica strain CCMP 1779 was purchased from the Culture Collection of Marine Phytoplankton (CCMP) and both *vde KO* and *lhcx1 KO* strains were previously generated (30).

Cultivation conditions. All microalgae strains of this work were cultivated according to ref. 51. They were maintained in F/2 solid media, with 32 g/L sea salts (Sigma Aldrich), 40 mM Tris-HCl (pH 8), Guillard's (F/2) marine water enrichment solution (Sigma Aldrich), and 1% agar (Duchefa Biochemie). Cells

Table 1. *Nannochloropsis* strains used in this work

Species	Strain	Reference
N. gaditana	WT	CCAP
	lhcx1 KO	(26, 50)
	ZEP OE	This work
	vde KO	This work
N. oceanica	WT	CCMP
	lhcx1 KO	(30)
	vde KO	(30)

were precultured in sterile F/2 liquid media in Erlenmeyer flasks irradiated with 100 μmol photons m^{-2} s^{-1}, 100 rpm agitation, at 22 ± 1 °C in a growth chamber.

In order to investigate xanthophyll accumulation dynamics in *N. gaditana*, cells were grown in a Multicultivator MC 1000-OD system (Photon Systems Instruments, Czech Republic) in liquid F/2 starting from 10 × 10^6 cells/mL, where constant air bubbling provides mixing and additional CO_2. Temperature was kept at 22 ± 1 °C and different light intensities were provided using an array of white LEDs.

Liquid cultures for phenotypic characterization and monitoring of photosynthetic functionality of the strains investigated in this work started from precultures grown in conditions described above. Cells were washed twice in fresh F/2 before starting growth curves from 5 × 10^6 cells/mL in F/2 supplemented with 10 mM $NaHCO_3$ to avoid carbon limitation, in Erlenmeyer flasks irradiated with 100 μmol photons m^{-2} s^{-1}, 100 rpm agitation, at 22 ± 1 °C in a growth chamber.

Semi-continuous growth was performed at 22 ± 1 °C in 5-cm Drechsel bottles, illuminated from one side, with 250 mL working volume. Mixing and carbon source was provided through the insufflation of air enriched with 5% CO_2 (v/v) at 1 L h^{-1}. In this case, F/2 growth media was enriched with added nitrogen, phosphate, and iron sources (0.75 g L^{-1} $NaNO_3$, 0.05 g L^{-1} NaH_2PO_4, and 0.0063 g L^{-1} $FeCl_3 \cdot 6H_2O$ final concentrations, respectively). Light was provided through cool white fluorescent lamps. Illumination rate was determined using the LI-250A photometer (Heinz-Walz, Effeltrich, Germany). Cultures were maintained in a semi-continuous mode diluting the culture every other day, as described in ref. 28. Cell concentrations were monitored before and after dilution with an automatic cell counter (Cellometer Auto X4, Cell Counter, Nexcelom). All experiments were conducted maintaining cell concentration at 250 × 10^6 cells mL^{-1} (~ 1.5 g L^{-1}) and exposing cultures to different light conditions: 400 and 1,200 μmol photons m^{-2} s^{-1} (*SI Appendix*, Fig. S1).

Biomass productivity. Biomass productivity of semi-continuous cultures was estimated by monitoring the dry weight of the culture in semi-continuous mode before and after dilution. Cultures were filtered using 0.45 μm filters, dried at 60 °C for 24 h, and weighed (28). To ensure that any residual inorganic material from the cultivation medium (e.g., inorganic salts) did not affect the dry-weight measurements, 5-mL microalgae samples were routinely diluted 1:5 with deionized water to dissolve inorganic salts before filtration.

High light treatment. High light treatments were performed using a LED Light Source SL 3500 (Photon Systems Instruments, Brno, Czech Republic). Cells were mixed in a thin cylinder placed in a water bath in order to get a homogeneous irradiance and a constant temperature.

Pigment Extraction. Total pigments were extracted using 1:1 ratio of 100% N, N-dimethylformamide (Sigma Aldrich), for at least 24 h, in the dark, at 4 °C (52). Absorption spectra were registered between 350 and 750 nm using a Cary 100 spectrophotometer (Agilent Technologies) to determine pigment concentration using specific extinction coefficients (52). Absorption values at 664 and 480 nm were used to calculate the concentrations of chlorophyll a and total carotenoids, respectively.

The content of individual carotenoids was determined after extraction with 80% acetone preceded by mechanical lysis using a Mini Bead Beater (Biospec Products) in the presence of glass beads (150 to 212 μm diameter, Sigma Aldrich), using a high-pressure liquid chromatography (HPLC) as previously described (53). The HPLC system consisted of a 139 reversed-phase column (5 μm particle size; 25 × 0.4 cm; 250/4 RP 18 Lichrocart, Darmstadt, Germany) and a diode-array detector to record the absorbance spectra (1,100 series, Agilent, 141 Waldbronn, Germany). The peaks of each sample were identified through the retention time and absorption spectrum (54). The vaucheriaxanthin absorption factor was estimated by correcting that of violaxanthin for their different absorption at 440 nm.

Fluorescence Measurements for the Monitoring of NPQ and Photosynthetic Functionality. The estimation of photosynthetic parameters was performed by measuring in vivo Chl fluorescence using a Dual PAM-100 fluorimeter (Heinz-Walz, Effeltrich, Germany). Samples were dark-adapted for 20 min, then exposed at 850 μmol photons m^{-2} s^{-1} (actinic light) and dark for different time frames to assess the activation and relaxation trends of NPQ in double kinetics (Fig. 2), respectively. For the phenotypic characterization of the strains investigated in this work, the samples were instead exposed to 2,000 μmol photons m^{-2} s^{-1} (actinic light) for 8 min and to dark for 15 min (Fig. 3). Photosynthetic functionality was monitored by treating samples at increasing irradiances of actinic light (*SI Appendix*, Fig. S5). In all protocols, saturating pulses and measuring light were set at 6,000 and 42 μmol photons m^{-2} s^{-1}, respectively. Maximum quantum yield of PSII (Φ_{PSII}), quantum yield of PSII in light-treated samples (Φ'_{PSII}), qL, and NPQ were calculated according to refs. 55 and 56.

Oxygen Evolution. Oxygen evolution was measured with a start-up O2K-Respirometer (NextGen-O2k and the PB-Module from Oroboros Instruments GmbH, Austria) in 2 mL samples at a concentration of 100 × 10^6 cells/mL in F/2 supplemented with 5 mM $NaHCO_3$ to avoid carbon limitation, in measuring chambers magnetically stirred at 750 rpm and with a frequency of 2 s. The light source was a blue LED with an emission peak at 451 nm (Osram Oslon). Instrument calibration was performed in the same medium and samples were dark-adapted for 10 min to assess respiration rate before starting the measurements of the oxygen flux at increasing irradiances. Respiration and photosynthesis rates were measured with the software DatLab 7.4.0.4.

Statistical Analysis. A statistical hypothesis testing was applied for all the data presented in this work, systematically comparing data from the parental strain with one single mutant line and at one single time point at a time. Statistical significance was assessed by *t* test using OriginPro 2020 (v. 9.7.0.188) (http://www.originlab.com/). Samples size was at least >4 for all the measurements collected in this work and for biomass productivity, it reached >10 data points for all strains investigated, and in some cases, the number of samples exceeded 30 (e.g., Fig. 5).

Data, Materials, and Software Availability. All study data are included in the article and/or *SI Appendix*.

ACKNOWLEDGMENTS. We acknowledge the support from Antoni Mateau Vera-Vives, Katarzyna Krawczyk, Andrea Meneghesso, Andrea Cailotto, and Matteo Scarsini for preliminary experiments. T. Morosinotto acknowledges the support from European Union H2020 Project 862087-GAIN4CROPS. D.L., S.W. and K.K.N. were supported by the U.S. Department of Energy, Office of Science, Basic Energy Sciences, Chemical Sciences, Geosciences, and Biosciences Division under field work proposal 449B. K.K.N. is an investigator of the Howard Hughes Medical Institute. We also acknowledge the UCB Vincent J. Coates Proteomics/Mass Spectrometry Laboratory (P/MSL), supported in part by NIH S10 Instrumentation Grant S10RR025622, for support in the mass spectrometry analysis.

Author affiliations: [a]Department of Biology, University of Padova, 35131 Padova, Italy; [b]Molecular Biophysics and Integrated Bioimaging Division, Lawrence Berkeley National Laboratory, Berkeley, CA 94720; [c]HHMI, University of California, Berkeley, CA 94720-3102; and [d]Department of Plant and Microbial Biology, University of California, Berkeley, CA 94720-3102

1. C. de Vargas *et al.*, Ocean plankton. Eukaryotic plankton diversity in the sunlit ocean. *Science* **348**, 1261605 (2015).
2. D. R. Ort *et al.*, Redesigning photosynthesis to sustainably meet global food and bioenergy demand. *Proc. Natl. Acad. Sci. U.S.A.* **112**, 8529–8536 (2015).
3. A. Alboresi, M. Storti, T. Morosinotto, Balancing protection and efficiency in the regulation of photosynthetic electron transport across plant evolution. *New Phytol.* **221**, 105–109 (2019).
4. Z. Li, S. Wakao, B. B. Fischer, K. K. Niyogi, Sensing and responding to excess light. *Annu. Rev. Plant Biol.* **60**, 239–260 (2009).
5. X. P. Li *et al.*, A pigment-binding protein essential for regulation of photosynthetic light harvesting. *Nature* **403**, 391–395 (2000).
6. G. Peers *et al.*, An ancient light-harvesting protein is critical for the regulation of algal photosynthesis. *Nature* **462**, 518–521 (2009).

7. R. C. Bugos, H. Y. Yamamoto, Molecular cloning of violaxanthin de-epoxidase from romaine lettuce and expression in Escherichia coli. *Proc. Natl. Acad. Sci. U.S.A.* **93**, 6320–6325 (1996).
8. P. Arnoux, T. Morosinotto, G. Saga, R. Bassi, D. Pignol, A structural basis for the pH-dependent xanthophyll cycle in Arabidopsis thaliana. *Plant Cell* **21**, 2036–2044 (2009).
9. M. Havaux, L. Dall'osto, R. Bassi, Zeaxanthin has enhanced antioxidant capacity with respect to all other xanthophylls in Arabidopsis leaves and functions independent of binding to PSII antennae. *Plant Physiol.* **145**, 1506–1520 (2007).
10. B. Demmig-Adams, J. J. Stewart, M. López-Pozo, S. K. Polutchko, W. W. Adams, Zeaxanthin, a molecule for photoprotection in many different environments. *Molecules* **25**, 5825 (2020).
11. C. Kulheim, J. Agren, S. Jansson, Rapid regulation of light harvesting and plant fitness in the field. *Science* **297**, 91–94 (2002).
12. S. P. Long *et al.*, Into the shadows and back into sunlight: Photosynthesis in fluctuating light. *Annu. Rev. Plant Biol.* **73**, 617–648 (2022).
13. L. Dall'Osto, S. Caffarri, R. Bassi, A mechanism of nonphotochemical energy dissipation, independent from PsbS, revealed by a conformational change in the antenna protein CP26. *Plant Cell* **17**, 1217–1232 (2005).
14. J. Kromdijk *et al.*, Improving photosynthesis and crop productivity by accelerating recovery from photoprotection. *Science* **354**, 857–861 (2016).
15. A. P. de Souza *et al.*, Soybean photosynthesis and crop yield is improved by accelerating recovery from photoprotection. *Science* **377**, 851–854 (2022).
16. R. Goss, B. Lepetit, Biodiversity of NPQ. *J. Plant Physiol.* **172**, 13–32 (2015).
17. R. Goss, D. Latowski, Lipid dependence of xanthophyll cycling in higher plants and algae. *Front. Plant Sci.* **11**, 455 (2020).
18. G. Perin, A. Bellan, A. Bernardi, F. Bezzo, T. Morosinotto, The potential of quantitative models to improve microalgae photosynthetic efficiency. *Physiol. Plant* **166**, 380–391 (2019).
19. E. Sforza, D. Simionato, G. M. Giacometti, A. Bertucco, T. Morosinotto, Adjusted light and dark cycles can optimize photosynthetic efficiency in algae growing in photobioreactors. *PLoS One* **7**, e38975 (2012).
20. L. Kalituho, J. Rech, P. Jahns, The roles of specific xanthophylls in light utilization. *Planta* **225**, 423–439 (2007).
21. H. Hartel, H. Lokstein, B. Grimm, B. Rank, Kinetic studies on the xanthophyll cycle in barley leaves (influence of antenna size and relations to nonphotochemical chlorophyll fluorescence quenching). *Plant Physiol.* **110**, 471–482 (1996).
22. L. Dall'Osto *et al.*, Two mechanisms for dissipation of excess light in monomeric and trimeric light-harvesting complexes. *Nat. Plants* **3**, 17033 (2017).
23. A. H. Short *et al.*, Xanthophyll-cycle based model of the rapid photoprotection of Nannochloropsis in response to regular and irregular light/dark sequences. *J. Chem. Phys.* **156**, 205102 (2022).
24. M. I. S. Naduthodi *et al.*, CRISPR-Cas ribonucleoprotein mediated homology-directed repair for efficient targeted genome editing in microalgae *Nannochloropsis oceanica* IMET1. *Biotechnol. Biofuels* **12**, 1–11 (2019).
25. Q. Wang *et al.*, Genome engineering of Nannochloropsis with hundred-kilobase fragment deletions by Cas9 cleavages. *Plant J.* **106**, 1148–1162 (2021).
26. A. Bellan, F. Bucci, G. Perin, A. Alboresi, T. Morosinotto, Photosynthesis regulation in response to fluctuating light in the secondary endosymbiont alga nannochloropsis gaditana. *Plant Cell Physiol.* **61**, 41–52 (2020).
27. B. Bailleul *et al.*, An atypical member of the light-harvesting complex stress-related protein family modulates diatom responses to light. *Proc. Natl. Acad. Sci. U.S.A.* **107**, 18214–18219 (2010).
28. G. Perin *et al.*, Cultivation in industrially relevant conditions has a strong influence on biological properties and performances of Nannochloropsis gaditana genetically modified strains. *Algal Res.* **28**, 88–99 (2017).
29. A. Meneghesso *et al.*, Photoacclimation of photosynthesis in the Eustigmatophycean Nannochloropsis gaditana. *Photosynth Res.* **129**, 291–305 (2016).
30. S. Park *et al.*, Chlorophyll–carotenoid excitation energy transfer and charge transfer in Nannochloropsis oceanica for the regulation of photosynthesis. *Proc. Natl. Acad. Sci. U.S.A.* **116**, 3385–3390 (2019).
31. S. Basso *et al.*, Characterization of the photosynthetic apparatus of the Eustigmatophycean Nannochloropsis gaditana: Evidence of convergent evolution in the supramolecular organization of photosystem I. *Biochim. Biophys. Acta* **1837**, 306–314 (2014).
32. J. S. Brown, Functional organization of chlorophyll a and carotenoids in the Alga, Nannochloropsis salina. *Plant Physiol.* **83**, 434–437 (1987).
33. L. M. Lubián *et al.*, Nannochloropsis (Eustigmatophyceae) as source of commercially valuable pigments. *J. Appl. Phycol.* **12**, 249–255 (2000).
34. E. Kress, P. Jahns, The dynamics of energy dissipation and xanthophyll conversion in Arabidopsis indicate an indirect photoprotective role of zeaxanthin in slowly inducible and relaxing components of non-photochemical quenching of excitation energy. *Front. Plant Sci.* **8**, 2094 (2017).
35. K. K. Niyogi, O. Bjorkman, A. R. Grossman, Chlamydomonas xanthophyll cycle mutants identified by video imaging of chlorophyll fluorescence quenching. *Plant Cell* **9**, 1369–1380 (1997).
36. J. M. Buck, P. G. Kroth, B. Lepetit, Identification of sequence motifs in Lhcx proteins that confer qE-based photoprotection in the diatom Phaeodactylum tricornutum. *Plant J.* **108**, 1721–1734 (2021).
37. T. Lacour, M. Babin, J. Lavaud, Diversity in xanthophyll cycle pigments content and related nonphotochemical quenching (NPQ) among microalgae: Implications for growth strategy and ecology. *J. Phycol.* **56**, 245–263 (2020).
38. L. Taddei *et al.*, Dynamic changes between two LHCX-related energy quenching sites control diatom photoacclimation. *Plant Physiol.* **177**, 953–965 (2018).
39. B. Lepetit *et al.*, The diatom Phaeodactylum tricornutum adjusts nonphotochemical fluorescence quenching capacity in response to dynamic light via fine-tuned Lhcx and xanthophyll cycle pigment synthesis. *New Phytol.* **214**, 205–218 (2017).
40. T. Morosinotto, R. Baronio, R. Bassi, Dynamics of chromophore binding to Lhc proteins in vivo and in vitro during operation of the xanthophyll cycle. *J. Biol. Chem.* **277**, 36913–36920 (2002).
41. A. Alboresi *et al.*, Conservation of core complex subunits shaped the structure and function of photosystem I in the secondary endosymbiont alga Nannochloropsis gaditana. *New Phytol.* **213**, 714–726 (2017).
42. M. Havaux, K. K. Niyogi, The violaxanthin cycle protects plants from photooxidative damage by more than one mechanism. *Proc. Natl. Acad. Sci. U.S.A.* **96**, 8762–8767 (1999).
43. S. Cazzaniga *et al.*, Domestication of the green alga Chlorella sorokiniana: Reduction of antenna size improves light-use efficiency in a photobioreactor. *Biotechnol. Biofuels* **7**, 157 (2014).
44. T. De Mooij *et al.*, Antenna size reduction as a strategy to increase biomass productivity: A great potential not yet realized. *J. Appl. Phycol.* **27**, 1063–1077 (2015), 10.1007/s10811-014-0427-y.
45. G. Perin, F. Gambaro, T. Morosinotto, Knowledge of regulation of photosynthesis in outdoor microalgae cultures is essential for the optimization of biomass productivity. *Front. Plant Sci.* **13**, 846496 (2022).
46. G. Perin, A. Bernardi, A. Bellan, F. Bezzo, T. Morosinotto, A mathematical model to guide genetic engineering of photosynthetic metabolism. *Metab. Eng.* **44**, 337–347 (2017).
47. S. Berteotti, M. Ballottari, R. Bassi, Increased biomass productivity in green algae by tuning non-photochemical quenching. *Sci. Rep.* **6**, 21339 (2016).
48. A. Garcia-Molina, D. Leister, Accelerated relaxation of photoprotection impairs biomass accumulation in Arabidopsis. *Nat. Plants* **6**, 9–12 (2020).
49. G. G. Lehretz, A. Schneider, D. Leister, U. Sonnewald, High non-photochemical quenching of VPZ transgenic potato plants limits CO_2 assimilation under high light conditions and reduces tuber yield under fluctuating light. *J. Integr. Plant Biol.* **64**, 1821–1832 (2022), 10.1111/JIPB.13320.
50. G. Perin *et al.*, Generation of random mutants to improve light-use efficiency of Nannochloropsis gaditana cultures for biofuel production. *Biotechnol Biofuels* **8**, 161 (2015).
51. A. Bellan, "Genetic engineering approaches to increase microalgae light use efficiency" (2018) (6 December 2022).
52. A. R. Wellburn, The spectral determination of chlorophylls a and b, as well as total carotenoids, using various solvents with spectrophotometers of different resolution. *J. Plant Physiol.* **144**, 307–313 (1994).
53. A. Färber, P. Jahns, The xanthophyll cycle of higher plants: Influence of antenna size and membrane organization. *Biochim. Biophys. Acta* **1363**, 47–58 (1998).
54. S. W. Jeffrey, R. F. C. Mantoura, S. W. Wright, "Phytoplankton pigments in oceanography: Guidelines to modern methods" in *Monographs on Oceanographic Methodology* (UNESCO, Paris, 1997).
55. K. Maxwell, G. N. Johnson, Chlorophyll fluorescence–A practical guide. *J. Exp. Bot.* **51**, 659–668 (2000).
56. N. R. Baker, Chlorophyll fluorescence: A probe of photosynthesis in vivo. *Annu. Rev. Plant Biol.* **59**, 89–113 (2008).